

Global three-dimensional flow of a neutron superfluid in a spherical shell in a neutron star

C. Peralta,^{1,2} A. Melatos,¹ M. Giacobello³ and A. Ooi³

cperalta@physics.unimelb.edu.au

ABSTRACT

We integrate for the first time the hydrodynamic Hall-Vinen-Bekarevich-Khalatnikov equations of motion of a 1S_0 -paired neutron superfluid in a rotating spherical shell, using a pseudospectral collocation algorithm coupled with a time-split fractional scheme. Numerical instabilities are smoothed by spectral filtering. Three numerical experiments are conducted, with the following results. (i) When the inner and outer spheres are put into steady differential rotation, the viscous torque exerted on the spheres oscillates quasiperiodically and persistently (after an initial transient). The fractional oscillation amplitude ($\sim 10^{-2}$) increases with the angular shear and decreases with the gap width. (ii) When the outer sphere is accelerated impulsively after an interval of steady differential rotation, the torque increases suddenly, relaxes exponentially, then oscillates persistently as in (i). The relaxation time-scale is determined principally by the angular velocity jump, whereas the oscillation amplitude is determined principally by the gap width. (iii) When the mutual friction force changes suddenly from Hall-Vinen to Gorter-Mellink form, as happens when a rectilinear array of quantized Feynman-Onsager vortices is destabilized by a counterflow to form a reconnecting vortex tangle, the relaxation time-scale is reduced by a factor of ~ 3 compared to (ii), and the system reaches a stationary state where the torque oscillates with fractional amplitude $\sim 10^{-3}$ about a constant mean value. Preliminary scalings are computed for observable quantities like angular velocity and acceleration as functions of Reynolds number, angular shear, and gap width. The results are applied to the timing irregularities (e.g., glitches and timing noise) observed in radio pulsars.

Subject headings: dense matter — hydrodynamics — stars: interior — stars: neutron — stars: rotation

¹School of Physics, University of Melbourne, Parkville, VIC 3010, Australia

²Departamento de Física, Escuela de Ciencias, Universidad de Oriente, Cumaná, Venezuela

³Department of Mechanical Engineering, University of Melbourne, Parkville, VIC 3010, Australia

1. Introduction

The global flow pattern in the superfluid interior of a neutron star is poorly known, yet it is a necessary input into global models of pulsar timing irregularities like glitches (Shemar & Lyne 1996; Lyne et al. 2000) and timing noise (Hobbs et al. 2002). The importance of the global dynamics was first demonstrated in pioneering laboratory experiments by Tsakadze & Tsakadze (1980), who impulsively accelerated rotating spherical and cylindrical containers filled with He II and observed abrupt changes in angular velocity, followed by intervals of prolonged relaxation, reminiscent of glitches observed in rotation-powered pulsars. The relaxation process can be interpreted as Ekman pumping following abrupt spin up (Alpar 1978; Anderson et al. 1978; Abney & Epstein 1996). The laminar, linear spin up of He II between two parallel plates was treated by Reisenegger (1993), who found a relation between the poloidal secondary flow and the torque on the container.

In this paper, we seek to determine which, if any, of the basic features of pulsar timing irregularities result directly from the nonlinear hydrodynamics (e.g., oscillations and instabilities) of the global flow. To do this, we solve numerically the Hall-Vinen-Bekarevich-Khalatnikov (HVBK) equations (Hall & Vinen 1956a,b; Bekarevich & Khalatnikov 1961) for a He-II-like superfluid contained in a differentially rotating spherical shell, building on previous numerical simulations of viscous spherical Couette flow in nonastrophysical settings (Marcus & Tuckerman 1987a,b; Dumas & Leonard 1994; Mamun & Tuckerman 1995).

Spherical Couette flow is controlled by two parameters: the aspect ratio (dimensionless gap width) δ , and the Reynolds number Re . In a slow rotator ($Re \ll 1$), the flow is axisymmetric. In a fast rotator ($Re \gg 1$), the flow is a combination of a primary azimuthal rotation and a secondary meridional circulation induced by Ekman pumping (Greenspan 1968). Transitions from the basic, null vortex state to single and twin vortex states can be triggered by gradually increasing Re above a critical value, producing abrupt changes in the rotation of the container. This has been observed numerically and experimentally in small ($\delta < 0.24$) and large ($\delta \geq 0.24$) gaps in ordinary fluids (Yavorskaya et al. 1975; Wimmer 1976; Tuckerman 1983; Sha & Nakabayashi 2001). Hollerbach (1998) also found evidence of time-dependent, asymmetric Taylor vortices, in medium gaps ($\delta = 0.336$). However, superfluid analogs of these experiments are hard to perform, partly because of problems with visualization techniques (Bielert & Stamm 1993). Numerical HVBK simulations have been performed in cylindrical Taylor-Couette geometries (Henderson et al. 1995; Henderson 2001; Henderson & Barenghi 2000), delivering good agreement with experiments, but not yet in the more challenging spherical Couette geometry. We attempt this here for the first time.

The paper is organized as follows. In §2, we establish the astrophysical context of our

numerical experiments by explaining how the idealized spherical Couette problem relates to a realistic neutron star. HVBK theory is reviewed in §3. The numerical method in spherical geometry is described and verified against test cases in §4. Results are then presented for the long-term response of the superfluid in three scenarios: the outer and inner spheres rotate steadily and differentially (§5), the outer sphere is accelerated impulsively (§6), and the mutual friction force changes suddenly (from anisotropic to isotropic form) in response to a line vortex instability (§7). Finally, in §8, we apply the results to pulsar timing irregularities and discuss the limitations of our approach.

2. Idealised hydrodynamic model of the outer core of a neutron star

In this paper, we conduct numerical experiments that seek to mimic, in an idealised context, the flow of neutron superfluid within the *outer core* of a rotating neutron star. The density of the outer core lies in the range $0.6\rho_* < \rho < 1.5\rho_*$, where $\rho_* = 2.6 \times 10^{14} \text{ g cm}^{-3}$ is the nuclear saturation density, which translates to radii in the range $5 \text{ km} \lesssim r \lesssim 9 \text{ km}$ (Sedrakian & Sedrakian 1995; Weber 1999; Yakovlev et al. 1999; Dean & Hjorth-Jensen 2003). We focus on the outer core because the superfluid is probably unpinned in this region (see below) —that is, it behaves essentially hydrodynamically— and its physical state is reasonably well understood, unlike the inner core. In the upper part of the outer core, $0.6\rho_* < \rho < \rho_*$, the neutrons form Cooper pairs in the 1S_0 state; in the lower part, $\rho_* < \rho < 1.5\rho_*$, they pair in the 3P_2 state (Weber 1999). Here, for simplicity, we assume that the isotropic 1S_0 phase fills the entire outer core. The 3P_2 phase is anisotropic: gradients in the orientation (texture) of the pair angular momenta drive counterflows between the viscous and inviscid components of the superfluid (Vollhard & Wölfle 2002; Mastrano & Melatos 2005), introducing complications (e.g. boundary conditions at the 1S_0 - 3P_2 interface) which lie outside the scope of this paper. ⁴

The outer core contains charged species, particularly protons and electrons, which are incorporated into the viscous component of the superfluid in our simulations. The protons are probably in a type II superconducting state, but the electrons are not (Sauls 1989). In a type II superconductor, the protons inside the magnetic fluxoids interact with the Feynman-Onsager vortices in the neutron superfluid, serving as natural pinning sites (Sauls 1989); the pinning geometry can be complicated (Ruderman et al. 1998) if the core magnetic

⁴A two-stream (Andersson et al. 2003) or Kelvin-Helmholtz (Mastrano & Melatos 2005) instability can be excited at the interface if the isotropic and anisotropic phases are in relative motion.

field has comparable poloidal and toroidal components (Thompson & Duncan 1993).⁵ We neglect this effect in what follows, as well as the effects arising from entropy gradients (Mastrano & Melatos 2005). In addition, the protons exert an effective drag on the neutrons by the so-called entrainment effect (Mendell 1991; Sedrakian & Sedrakian 1995), in which the momentum of one species is partly carried along by the other species, as in ${}^3\text{He}$ - ${}^4\text{He}$ mixtures (Andreev & Bashkin 1976; Andersson & Comer 2001). We neglect this effect in the computations in this paper, where there is no entropy gradient at the 3P_2 - 1S_0 interface (Mastrano & Melatos 2005).

The hydrodynamic boundary conditions at the upper and lower surfaces of the outer core are set by the conditions in the inner crust and inner core respectively. The physical state of the inner core is essentially unknown, so we experiment with the two extremes of rough walls (pinning) and perfect slip (no pinning) at this boundary. For example, pinning is favored if triple-flavor color superconductivity results in a crystal lattice in the inner core (Rajagopal 2002). In the inner crust, it is widely believed that the Feynman-Onsager vortices are trapped at nuclear pinning sites (Sauls 1989), so that a rough wall is the appropriate boundary condition. However, recent work suggests that, even in the inner crust, pinning may not occur. Donati & Pizzochero (2003) studied the vortex-nucleus interaction and found interstitial pinning only, with low pinning forces $\lesssim 0.4 \text{ MeV fm}^{-1}$.

In the standard picture of pulsar glitches, the stellar crust is loosely coupled to a rapidly rotating superfluid interior (Lyne & Graham-Smith 1998). Although we do not attempt to explicitly construct a model of glitches in this paper, our simulations address a similar scenario: the upper and lower surfaces of the outer core rotate differentially, as the crust spins down electromagnetically, until a glitch occurs and the crust suddenly accelerates. We study the global superfluid flow pattern in the outer core before and after the glitch. We also study how the Feynman-Onsager vortices switch from a rectilinear array to a reconnecting tangle via the Donnelly-Glaberson instability (Glaberson et al. 1974). The transition from an organized to a disorganized distribution of superfluid vorticity in the outer core, together with the acceleration of the crust, strongly affects the rotation of the star, as we show below.

⁵Pinning in the outer core is arguably inconsistent with the precession periods ($\sim 1 \text{ yr}$) observed in some pulsars (Stairs et al. 2000), because the Feynman-Onsager vortices damp the precession on short time scales ($\sim 1 \text{ hr}$) as they pass through the array of magnetic fluxoids (Link 2003).

3. HVBK theory

HVBK theory is a generalization of the two-fluid Landau-Tisza theory for superfluid He II that includes the physics of quantized Feynman-Onsager vortices (Hall & Vinen 1956a,b; Bekarevich & Khalatnikov 1961). It applies equally well to a neutron superfluid with 1S_0 parity (Tilley & Tilley 1986). Fluid particles in the theory are assumed to be threaded by many coaligned vortices. In the continuum limit, we can define a macroscopic superfluid vorticity $\omega_s = \nabla \times \mathbf{v}_s$ which is not zero, despite the fact that, microscopically, the superfluid obeys $\nabla \times \mathbf{v}_s = 0$. This is valid if the length scales in the flow are longer than the average separation between vortex lines. The isothermal HVBK equations of motion take the form (Barenghi & Jones 1988; Henderson & Barenghi 2000)

$$\frac{d_n \mathbf{v}_n}{dt} = -\frac{\nabla p_n}{\rho} + \nu_n \nabla^2 \mathbf{v}_n + \frac{\rho_s}{\rho} \mathbf{F} - \frac{\rho_s \nu_s}{\rho} \nabla |\omega_s|, \quad (1)$$

$$\frac{d_s \mathbf{v}_s}{dt} = -\frac{\nabla p_s}{\rho} + \nu_s \mathbf{T} - \frac{\rho_n}{\rho} \mathbf{F} - \frac{\rho_s \nu_s}{\rho} \nabla |\omega_s|, \quad (2)$$

with $d_{n,s}/dt = \partial/\partial t + \mathbf{v}_{n,s} \cdot \nabla$, supplemented by the incompressibility condition $\nabla \cdot \mathbf{v}_n = \nabla \cdot \mathbf{v}_s = 0$, a good approximation in a neutron star, where the flow is subsonic. In (1) and (2), $\mathbf{v}_{n,s}$ and $\rho_{n,s}$ are the normal fluid and superfluid velocities and densities respectively. Effective pressures p_s and p_n are defined by $\nabla p_s = \nabla p - \frac{1}{2} \rho_n \nabla(\mathbf{v}_{ns}^2)$ and $\nabla p_n = \nabla p + \frac{1}{2} \rho_s \nabla(\mathbf{v}_{ns}^2)$, with $\mathbf{v}_{ns} = \mathbf{v}_n - \mathbf{v}_s$. We define ν_n to be the kinematic viscosity of the normal fluid and $\nu_s = (\kappa/4\pi) \log(b_0/a_0)$ to be the stiffness parameter, where $\kappa = h/2m_n$ is the quantum of circulation, m_n is the mass of the neutron, a_0 is the radius of the vortex core, and b_0 is the intervortex spacing. Note that ν_s has the same dimensions as a kinematic viscosity but controls the oscillation frequency of Kelvin waves excited on the vortex lines (Henderson et al. 1995).

The vortex tension force per unit mass, $\nu_s \mathbf{T}$, is given by

$$\mathbf{T} = \omega_s \times (\nabla \times \hat{\omega}_s), \quad (3)$$

with $\hat{\omega}_s = \omega_s/|\omega_s|$. The tension arises from local circulation around quantized vortex lines. It corresponds to the Magnus self-force exerted on a line by its own, self-induced velocity field, which is given by $\nu_s \omega_s \times (\nabla \times \hat{\omega}_s)$ in the local induction approximation of the full Biot-Savart integral, when the radius of curvature is much larger than a_0 (Donnelly 1991).

The mutual friction force per unit mass arises from the interaction between the quantized vortex lines and the normal fluid (via roton scattering in He II and electron scattering in a neutron star) (Hall & Vinen 1956a,b). The form of this force depends on the global

configuration of the vortices. If the vortices occupy a rectilinear array, the friction force per unit mass takes the Hall-Vinen (HV) form (Hall & Vinen 1956a,b)

$$\mathbf{F} = \frac{1}{2}B\hat{\omega}_s \times (\omega_s \times \mathbf{v}_{ns} - \nu_s \mathbf{T}) + \frac{1}{2}B'(\omega_s \times \mathbf{v}_{ns} - \nu_s \mathbf{T}) \quad (4)$$

where B and B' are dimensionless, temperature-dependent coefficients (Barenghi et al. 1983). However, in a realistic neutron star, the distribution of vorticity need not correspond to a rectilinear vortex array (Greenstein 1970, 1974). For example, differential rotation can trigger the Donnelly-Glaberson (DG) instability (Cheng et al. 1973; Glaberson et al. 1974), in which a dense tangle of vortices forms in the counterflow. Experimental evidence for this effect comes from counterflow experiments that measure the attenuation of second sound in narrow channels (Vinen 1957; Swanson et al. 1983), supported by numerical simulations using the vortex filament method (Tsubota et al. 2003). From these experiments, it is inferred that the friction force per unit mass takes the isotropic Gorter-Mellink (GM) form (Gorter & Mellink 1949)

$$\mathbf{F} = A' \left(\frac{\rho_n \rho_s v_{ns}^2}{\kappa \rho^2} \right) \mathbf{v}_{ns}, \quad (5)$$

where $A' = B^3 \rho_n^2 \pi^2 \chi_1^2 / 3 \rho^2 \chi_2^2$ is a dimensionless, temperature-dependent coefficient, related to the original GM constant (usually denoted as A in the literature) by $A' = A \rho \kappa$. Here, χ_1 and χ_2 are dimensionless constants of order unity (Vinen 1957). Note that (1) and (2), derived assuming a dense, roughly parallel array of vortices, may not be consistent with (5). The validity of HVBK theory in turbulent flow is yet to be established (Barenghi et al. 1995).

4. Numerical Method

4.1. Pseudospectral collocation in spherical geometry

Equations (1) and (2) are discretized in space using a pseudospectral collocation method (Canuto et al. 1988). A time-split fractional step algorithm advances the solution (Canuto et al. 1988; Bell & Colella 1989; Streett & Hussaini 1991). Nonlinear terms are treated explicitly using a third-order Adams-Bashforth scheme and diffusive terms are treated implicitly using a Crank-Nicholson scheme (Boyd 2001). Incompressibility is enforced by pressure-correction projection (Brown et al. 2001; Chorin 1968). We follow closely the approach of Bagchi & Balachandar (2002), expanding the polar (θ) and azimuthal (ϕ) coordinates in Fourier functions and the radial (r) coordinate in Chebyshev polynomials. The velocity fields are expressed as $u(r, \theta, \phi) = \sum_{i,j,k} C_{ijk} T_i(r) f(j\theta) e^{ik\phi}$, where $T_i(r)$ is the i -th Cheby-

shev polynomial, $f(\theta)$ equals $\sin \theta$ or $\cos \theta$, and i, j, k are integers running from 0 to N_r, N_θ, N_ϕ respectively. The pole parity problem which plagues Fourier series on a sphere (Boyd 2001) must be handled with care; the tangential and azimuthal components of \mathbf{v}_n and \mathbf{v}_s change sign across the poles (Orszag 1974; Fornberg 1998).

Spectral methods are global and therefore sensitive to boundary conditions. The normal fluid \mathbf{v}_n satisfies no-slip and no-penetration boundary conditions at the inner and outer surfaces of the container. There is no general agreement in the literature on what boundary conditions are suitable for \mathbf{v}_s . Khalatnikov (1965) suggested that vortex lines can either slide along, or pin to, the boundaries. The tangential velocity \mathbf{v}_L of a vortex line relative to a rough boundary is given by (Hills & Roberts 1983)

$$(\mathbf{n} \cdot \boldsymbol{\omega}_s)\boldsymbol{\omega}_s \times \mathbf{v}_L = 0, \quad (6)$$

where \mathbf{n} is the unit normal to the surface; in this case, vortex lines are permanently attached to the surface. At a smooth boundary, on the other hand, one has

$$(\mathbf{n} \cdot \boldsymbol{\omega}_s)\boldsymbol{\omega}_s \times \mathbf{n} = 0; \quad (7)$$

in this case, vortex lines are oriented perpendicular to the surface. Condition (6) is difficult to implement in HVBK theory, in which each fluid element is threaded by many vortex lines, because \mathbf{v}_L cannot be calculated from \mathbf{v}_n and \mathbf{v}_s . On the other hand, frictionless sliding ($\boldsymbol{\omega}_s \times \mathbf{n} = 0$) leads to numerical instabilities, because $\boldsymbol{\omega}_s$ can develop parallel components near the surface as it evolves (Henderson & Barenghi 2000). Therefore, in this paper, we adopt no-slip and no-penetration [i.e., pinning; see Baym et al. (1992)] boundary conditions for \mathbf{v}_s to stabilize the evolution.

Spectral methods can develop global oscillations, due to the Gibbs phenomenon, when applied to problems with stiff numerical solutions or discontinuities (Vandeven 1991). In the superfluid, such oscillations are damped indirectly (and weakly) through \mathbf{F} . To mitigate this problem, we filter out high spatial frequency modes in the r and θ expansions by multiplying the spectral coefficients by an exponential filter defined by $\sigma_e(k/N_{r,\theta}) = \exp[-(k/N_{r,\theta})^\gamma \ln \epsilon]$, with $0 \leq |k| \leq N_{r,\theta}$, where $\epsilon = 2.2 \times 10^{-16}$ is the machine zero and γ is the order of the filter. Strong filtering is needed ($\gamma \leq 8$) in order to stabilize the evolution. Most of our runs employ grids with $(N_r, N_\theta, N_\phi) = (210, 250, 4)$, although a few have $N_\phi = 32$.

As our simulations are the first to treat the spherical Couette problem for superfluids, we are obliged to validate the code in the simpler case of a classical viscous fluid. In this limit ($\rho_s \rightarrow 0, \rho_n \rightarrow \rho$ as $T \rightarrow T_c$), we successfully reproduce the $0 \rightarrow 1$ and $1 \rightarrow 2$ vortex-state transitions observed in small and large gaps in spherical Couette flow (Marcus & Tuckerman

1987a,b; Dumas & Leonard 1994), achieving agreement to three significant digits in the critical value of Re and nine significant digits in the torque.

4.2. Model pulsar

Our model pulsar consists of a spherical shell filled with a 1S_0 -paired neutron superfluid. The inner (radius R_1) and outer (radius R_2) surfaces of the shell rotate at angular velocities Ω_1 and Ω_2 , respectively, about a common axis. Henceforth, all quantities are expressed in dimensionless form using R_2 as the unit of length and Ω_1^{-1} as the unit of time. The Reynolds number and dimensionless gap width are defined by $Re = \Omega_1 R_2^2 / \nu_n$ and $\delta = (R_2 - R_1) / R_2$ respectively.

Our choice of parameters is limited by computational capacity. For example, in a realistic pulsar, one might expect $10^{-9} \lesssim \Delta\Omega / \Omega \lesssim 10^{-6}$ in the lead-up to a glitch (Hobbs 2002), with $\Delta\Omega = |\Omega_2 - \Omega_1|$. We take $0.1 \leq \Delta\Omega \leq 0.3$ instead, in order to observe the long-term effect of differential rotation (i.e., several full “wraps” of the inner sphere relative to the outer sphere) over a time interval $0 \leq t \leq 90$ that is computationally achievable.

Initially, both fluids must satisfy the incompressibility condition, with $(\mathbf{v}_n)_r = (\mathbf{v}_s)_r = 0$ at $r = R_1, R_2$. We choose the Stokes solution (Landau & Lifshitz 1963) as the initial condition, with $\mathbf{v}_s = \mathbf{v}_n$. We also take $\rho_s / \rho = 0.908$ and $\rho_n / \rho = 0.092$, corresponding to the superfluid and normal fluid fractions in He II at a fiducial temperature $T/T_c = 0.66$ (in a realistic pulsar, one has $T/T_c \lesssim 0.1$). Importantly, the Reynolds number in a typical neutron star can reach $Re \sim 10^{11}$ (Mastrano & Melatos 2005), whereas, in our simulations, we restrict ourselves to $10^2 \leq Re \leq 10^4$ for two reasons: for $Re \geq 10^5$, the normal fluid flow becomes turbulent, and we cannot resolve it properly; and, when Re is smaller, a steady state is reached in a shorter time.

We set the stiffness parameter to $\nu_s = 10^{-5} \text{ cm}^2\text{s}^{-1}$, such that $\nu_s \ll \nu_n$ as in a young pulsar (Greenstein 1970), even though a more realistic value is $\nu_s = 10^{-3} \text{ cm}^2\text{s}^{-1}$ [cf. $\nu_n \approx 10^2 \text{ cm}^2\text{s}^{-1}$; Mastrano & Melatos (2005)]. In practice, ν_s cannot be chosen independently of δ . For a small gap ($\delta < 0.1$) or large ν_s , the tension force disrupts the flow and leads to numerical instabilities, in which the stiff superfluid streamlines bend sharply at the walls. This effect is suppressed in a cylindrical shell, where the tension causes the superfluid to rotate as a column parallel to the curved walls (Henderson & Barenghi 2000). Consequently, perfect slip boundary conditions on \mathbf{v}_s may prove beneficial in the spherical problem; we will investigate them in a future paper.

The HV friction force parameters B and B' are unknown in a neutron star. We choose

$B = 1.35$ and $B' = 0.38$, adopting the He II values at $T/T_c = 0.66$ (Barenghi et al. 1983; Donnelly 1991; Donnelly & Barenghi 1998). The parameter $A' = 5.8 \times 10^{-3}$ (with $\chi_1/\chi_2 = 0.3$) at the same temperature can be calculated from a fitting formula derived by Dimotakis (1972), which is consistent with previously published experimental values (Vinen 1957). Stable long-term evolution is difficult to achieve for this value of A' , so we take $A' = 5.8 \times 10^{-2}$ instead. A more detailed study of the dynamics for a wider range of B , B' and A' will be presented in a forthcoming paper.

5. Steady differential rotation

In this section, we describe the results of a control experiment in which the the inner and outer spheres rotate steadily yet differentially, i.e., Ω_1 and $\Omega_2 \neq \Omega_1$ are held constant. We consider four cases, identified by Au, Bu, Cu, and Du in Table 1, corresponding to medium and large gaps ($\delta = 0.5, 0.3$) and small and medium shear ($0.7 \leq \Omega_2 \leq 0.9$). A few preliminary runs with $N_\phi = 32$ confirm that the flow remains axisymmetric, so we restrict the resolution to $(N_r, N_\theta, N_\phi) = (150, 400, 4)$ in what follows.

Figure 1 displays the meridional streamlines of the normal fluid and the superfluid for $\delta = 0.3$ and $\Delta\Omega = 0.3$ as a function of time. The corresponding torques on the inner and outer spheres are plotted as dashed curves in Figures 2a and 2b respectively, with squares marking the instants when the streamlines are plotted in Figure 1. The torque oscillates quasi-periodically, with a final periodic state that persists as long as the differential rotation is maintained (up to $t = 90$ in our runs), with a peak-to-peak fractional amplitude $\Delta N_z/N_z \approx 0.02$. The flow pattern in the normal fluid contains a secondary vortex near the poles for $8 \leq t < 20$, which expands and contracts quasi-periodically. For $t > 20$, the secondary vortex disappears and a single meridional shell remains, which also expands and contracts, but only slightly. The superfluid streamlines display a richer pattern: an equatorial vortex develops at $6 \leq t \leq 8$, a polar vortex develops at $8 \leq t \leq 20$, and the mid-latitude flow becomes disorganized for $t \geq 20$. Note that we must reduce the spatial resolution to $(N_r, N_\theta) = (120, 250)$ during the run in order to stabilize the evolution; for $(N_r, N_\theta) = (150, 400)$, one observes sudden jumps in the torque unless $\Delta t \leq 10^{-5}$ (which lengthens the runs unacceptably). It is possible that turbulence is generated in \mathbf{v}_s for $t \geq 20$ and that, by intentionally choosing a coarser resolution, we are effectively smoothing over the turbulent eddies.

The torque evolves similarly in all four cases. Initially, the linear Stokes solution adjusts to a nonlinear, cellular solution (with meridional circulation) within a time $\Delta t \sim 6$. This transient state is of no interest astrophysically. Subsequently, the torque oscillates persis-

tently —a new and astrophysically relevant phenomenon. The oscillation amplitude depends strongly on the gap width δ and weakly on the shear $\Delta\Omega$. For example, if $\delta = 0.5$ is held constant, the amplitude decreases from $\Delta N_z/N_z = 0.026$ to $\Delta N_z/N_z = 0.014$ as the shear decreases from $\Delta\Omega = 0.3$ (solid curve in Figure 2) to $\Delta\Omega = 0.1$ (dotted curve in Figure 2). On the other hand, if $\Delta\Omega = 0.3$ is held constant, the amplitude decreases from 0.036 to 0.026 as δ increases from 0.3 to 0.5 (dashed and solid curves in Figure 2).

6. Impulsive acceleration of the outer sphere

When a glitch is triggered in a rotation-powered pulsar, the crust and consequently the superfluid interior are spin up impulsively. We simulate a spin-up event of this kind by abruptly accelerating the rotation of the outer sphere from $0.7 \leq \Omega_2 \leq 0.9$ to $\Omega_2 = 1$ at $t = 20$. Figure 3a shows the change in the flow pattern of the normal fluid and superfluid before and after this sudden acceleration. The difference is more pronounced in the normal fluid; a secondary vortex appears at mid-latitudes in each hemisphere, adjacent to the outer shell. The jump in torque comes almost entirely from these mid-latitude regions.

Figure 1b shows how the dominant spectral coefficients C_{ijk} ($k = 1$) of $(\mathbf{v}_n)_\theta$ behave before and after the spin-up event. The three modes of highest amplitude before acceleration are $C_{221} > C_{421} > C_{521}$. After acceleration, the same ordering is observed, but with amplitudes $\approx 12\%$ lower, and the fourth-strongest mode switches from C_{621} to C_{321} . By contrast, in similar data for $(\mathbf{v}_s)_\theta$, no change is seen in the ordering of the top 10 spectral coefficients, and their amplitudes change by less than 10%. The superfluid is therefore largely unaffected by the glitch, as one might anticipate by inspecting Figure 3; most of the effect is transmitted to the normal fluid by the viscous Ekman layer adjacent to the outer shell.

A key numerical issue is whether the spectral method faithfully resolves the flow. Empirically, this occurs if the mode amplitudes decrease quasi-monotonically with polynomial index. We confirm this here. The Chebyshev modes, plotted in Figure 4, decrease by a factor $\sim 10^4$ in amplitude from $i = 1$ to $i = 50$, indicating that the flow is resolved in r . We also increase the resolution in ϕ at $t > 20$ by Fourier interpolation and confirm that the results are identical for $4 \leq N_\phi \leq 32$.

When the outer sphere is accelerated, we find that the time-step must be halved to avoid sudden artificial jumps in the torque. This property has been noted widely in the literature: in viscous spherical Taylor-Couette flow, the nonlinear dynamics depends sensitively on the time-step in the transition between different vortex states (Loukopoulos & Karahalios 2004; Sha & Nakabayashi 2001; Liu et al. 1996). For example, Loukopoulos & Karahalios (2004)

reported that the transition to an asymmetric 1-vortex state can only be achieved by varying Re quasi-statically near its critical value and using a small ($\Delta t = 10^{-4}$) time step. Different flow states in viscous spherical Couette flow are associated with energy differences. If the system is driven through an intermediate state too quickly, the flow cannot follow the fast change, due to its inertia, and a steady final state cannot be reached (Wimmer 1976).

The post-acceleration evolution of the torque is qualitatively similar in the four cases studied. This can be observed in Figure 5, where we plot the fractional change in the angular velocity $\Delta\Omega/\Omega$ and its first time derivative $\Delta\dot{\Omega}/\dot{\Omega}$ as a function of time.⁶ In radio pulsars, both these quantities are observed to high accuracy in radio timing experiments. The outer torque jumps at $t = 20$, oscillates with a period $\Delta t \sim 5$, then decays quasi-exponentially. Note that, in Figure 5b, the curves for Aa, Ca and Da are grouped together quite closely before acceleration, whereas the curves for Aa and Ba are grouped closely after acceleration. This implies that the gap width δ is the main parameter controlling the spin-down torque over the long term (i.e., during steady differential rotation), as in §5, whereas the angular velocity jump $|\Omega_2 - \Omega_1|$ is the main parameter controlling the relaxation time-scale. By fitting an exponential to the secular evolution of $\Delta\dot{\Omega}$, we find that the (e^{-1}) relaxation time-scale is given by $\tau = 12, 9.5, 9.3,$ and 8.2 for Aa, Ba, Ca, and Da respectively and scales roughly as $\tau \propto \delta^{1/3}|\Omega_2 - \Omega_1|^{1/3}$, similar to (but not exactly the same as) the Ekman scaling $\tau \propto |\Omega_2 - \Omega_1|^{1/2}$.

7. Instability of the Vortex Array

The stability of a rectilinear array of quantized vortices was investigated by Vinen in counterflow experiments in narrow channels (Vinen 1957). He attributed the attenuation of second sound to the generation of a “vortex tangle” in the counterflow. The critical (axial) counterflow velocity v_{ns} for the onset of this turbulent state was calculated theoretically by Glaberson et al. (1974), for small perturbations of a single vortex line (Cheng et al. 1973). He found that, for $v_{ns} > 2(2\Omega\nu_s)^{1/2}$, growing Kelvin waves are excited and the vortex lines reconnect to form a tangle, in accord with experimental data (Cheng et al. 1973). Similar results have been produced by numerical simulations with the vortex filament method (Schwarz 1988; Tsubota et al. 2003). The inclusion of slow rotation in counterflow experiments reduces the critical v_{ns} at which superfluid turbulence sets in (Swanson et al.

⁶Note that $\Omega_2(t)$ is held fixed in the code after the acceleration at $t = 20$. Hence the angular velocity change $\Delta\Omega = \Omega_2(t) - \Omega_2(20)$ plotted in Figure 5 is not computed self-consistently. It is found by integrating the viscous torque on the outer sphere, calculated by solving (1) and (2) subject to the time-independent boundary condition $\Omega_2(t) = \text{constant}$.

1983).

In order to simulate what happens when a vortex tangle develops from an initially regular vorticity distribution, we suddenly change the friction force in (1) and (2) from HV to GM form, according to the prescription in §4. From Figure 6, we observe that the torque reaches a stationary state ~ 3 times more quickly than in the spin-up experiments presented in §6. The torque decays more quickly than an exponential, as can be appreciated from Figure 6. Nevertheless, we can estimate the (e^{-1}) relaxation time-scale for the cases Af, Bf, Cf, and Df in Table 1 to be 3.4, 3.4, 3.0, and 3.6, respectively. The relaxation time is essentially independent of δ and $|\Omega_2 - \Omega_1|$.

Relaxation occurs more quickly than in the spin-up experiment because the GM force is small compared to the HV force. From §6, we have $|\mathbf{F}_{\text{GM}}|/|\mathbf{F}_{\text{HV}}| = (A'/B)(\rho_n\rho_s/\rho^2)(v_{ns}^2/\kappa\omega_s)$ [and hence $\propto (\rho_n/\rho)^3$ for $\rho_n \ll \rho$]; on the other hand, we find $|\mathbf{F}_{\text{GM}}|/|\mathbf{F}_{\text{HV}}| \approx 10^{-5}$ empirically from our runs, implying $v_{ns}^2/\kappa\omega_s \approx 2.2 \times 10^{-6}$. The sudden change in the mutual friction effectively uncouples the normal fluid and the superfluid, and the torque evolves rapidly to a constant value on a time-scale $\Delta t \sim 3$. After this time, the inner and outer torques are equal to one part in $\sim 10^3$ and their mean values hardly vary at all. Nevertheless, while the torque appears constant for $t > 25$ in Figure 6, closer examination on a magnified scale shows that $|N_2 - N_1|$ oscillates persistently, out to $t = 90$, with peak-to-peak amplitude $\Delta N_z/N_z \sim 10^{-3}$.

8. Discussion

In this paper, we present the first three-dimensional hydrodynamic HVBK simulations of a 1S_0 -paired neutron superfluid in a rotating spherical shell, generalizing studies of viscous fluids in spherical Couette geometry (Marcus & Tuckerman 1987a,b; Dumas & Leonard 1994) and He II in cylindrical Couette geometry (Henderson et al. 1995; Henderson & Barenghi 2000). The code accurately resolves the superfluid flow pattern for Reynolds numbers and gap widths in the range $10 \leq Re \leq 10^4$ and $0.2 \leq \delta \leq 0.7$, respectively.

Persistent quasiperiodic oscillations are always observed in the torque during steady differential rotation, after the initial transient dies away, with typical period $\sim \Omega_1^{-1}$ and fractional amplitude $\sim 10^{-2}$. The oscillation amplitude increases as Re increases. The gap width δ principally controls the spin-down torque over the long term, during steady differential rotation, whereas the frequency jump $|\Omega_2 - \Omega_1|$ principally sets the relaxation time-scale after a sudden acceleration of the outer sphere. If, instead of spinning up the outer sphere, we suddenly switch the mutual friction force from anisotropic (HV) form to

isotropic (GM) form, as happens when a rectilinear array of quantized vortices reconnects unstably to form a tangle, the relaxation time-scale is ~ 3 times shorter and the torque difference $|N_2 - N_1|$ oscillates subsequently with peak-to-peak fractional amplitude $\sim 10^{-3}$ around a constant mean value. We speculate that a transition from a turbulent flow, driven by long-term differential rotation, to a laminar flow immediately after a glitch, might cause some of the timing irregularities observed in pulsars. Similar transitions from turbulent to laminar flow in a superfluid have already been observed in laboratory experiments where He II, cooled to a few mK, flows around an oscillating microsphere (Niemetz et al. 2002; Schoepe 2004).

Computational limitations impose upon us some artificial approximations. Some of these approximations will be tested independently in a future paper. For example, one might hope to use a weaker filter when damping the high spatial frequency modes, perhaps by introducing an artificial viscosity (Andreassen et al. 1994; Ould Kaber 1996), and one can model small-scale turbulence using the techniques of large eddy simulations (Germano et al. 1991; Lilly 1992; Mahesh et al. 2004). Moreover, although some of our parameters are not as close as one might wish to realistic neutron star values, we are careful to respect the ordering of physical quantities encountered in a neutron star (e.g., $\Delta\Omega_2 \ll \Omega_2$, $Re \gg 1$, $\nu_s \ll \nu_n$) and to use values of the dimensionless friction coefficients (B , B' and A') that apply to the neutron star regime $\rho_n \ll \rho_s$ and are consistent with experimental data on He II. By artificially reducing ν_s by two orders of magnitude, we trade off some accuracy for computational speed in our modeling of old pulsars, where the tension force is the primary interaction (Greenstein 1970), although our modeling of young pulsars is mostly unimpaired (Hobbs et al. 2004; Lyne et al. 2000).

We consider superfluid flow in the outer core of the star, where there is no pinning in the body of the fluid, only at the boundary. Consequently, those parts of our analysis pertaining to the formation of a reconnecting vortex tangle via the DG instability may not translate straightforwardly to the inner crust, where pinning at multiple lattice sites along a vortex line may suppress the DG instability and even prevent a tangle from forming at all. On the other hand, if Ekman pumping is the primary core-crust coupling mechanism in a real neutron star, then the dynamics in the outer core must dominate the physics; crust-only mechanisms are inconsistent with observations of Vela’s glitches in the Ekman regime (McCulloch et al. 1990; Abney et al. 1996).

The time-scales of torque fluctuations in our numerical experiments are generally $\lesssim 10\Omega_1^{-1}$, much shorter than the time-scales for post-glitch relaxation and timing noise oscillations observed in radio pulsars. However, it is crucial to realize that the numerical time-scales will lengthen greatly in more realistic simulations, where the angular shear is lower and Re is

higher. Such numerical experiments are computationally challenging, and we are investigating alternative numerical approaches that may render them tractable.

A necessary extension of the code is to include radial stratification. It has been argued that, for a viscous fluid, stratification hampers the formation of an Ekman layer near the outer boundary (Abney & Epstein 1996). The Brunt-Väisälä frequency in a neutron star was estimated to be $\omega_{\text{BV}} \sim 500\text{s}^{-1}$ around nuclear density and $\omega_{\text{BV}} \sim 0.7\Omega_2$ for the Vela pulsar (Reisenegger & Goldreich 1992), whereas one needs $\omega_{\text{BV}} \lesssim 0.2\Omega_2$ for Ekman pumping to proceed effectively (Abney & Epstein 1996). Stratification can also affect the coupling between the crust and the superfluid core of a neutron star by modifying precessional modes (Levin & D’Angelo 2004). The pressure projection operation in our code relies on incompressibility, so stratification is hard to include self-consistently. As a first approximation, however, one can set $v_r = 0$ in the incompressible calculation, as proposed by Levin & D’Angelo (2004).

The HVBK equations may not apply to a vortex tangle. An alternative theory which explicitly treats displacements and oscillations of the vortex array was developed by Chandler & Baym (1983, 1986). The complexities thereby introduced, and fresh uncertainties over boundary conditions, raise new numerical challenges.

We acknowledge the computer time supplied by the Australian Partnership for Advanced Computation (APAC) and the Victorian Partnership for Advanced Computation (VPAC). We also thank George Hobbs for helpful discussions and Caroline Andrzejewski for undertaking a thorough literature review of spherical Couette flow in support of this research.

REFERENCES

- Abney, M., & Epstein, R. I. 1996, *J. Fluid Mech.*, 312, 327
- Abney, M., Epstein, R. I., & Olinto, A. V. 1996, *ApJ*, 466, L91+
- Alpar, M. A. 1978, *J. Low Temp. Phys.*, 31, 803
- Anderson, P. W., Pines, D., Ruderman, M., & Shaham, J. 1978, *J. Low Temp. Phys.*, 30, 839
- Andersson, N., & Comer, G. L. 2001, *Physical Review Letters*, 87, 241101
- Andersson, N., Comer, G. L., & Prix, R. 2003, *Physical Review Letters*, 90, 091101

- Andreassen, O., Lie, I., & Wasberg, C. E. 1994, *Journal of Computational Physics*, 110, 257
- Andreev, A. F., & Bashkin, E. P. 1976, *Sov. Phys. JETP*, 42, 164
- Bagchi, B., & Balachandar, S. 2002, *J. Fluid. Mech.*, 466, 365
- Barenghi, C. F., Donnelly, R. J., & Vinen, W. F. 1983, *J. Low Temp. Phys.*, 52, 189
- Barenghi, C. F., & Jones, C. A. 1988, *J. Fluid Mech.*, 197, 551
- Barenghi, C. F., Swanson, C. J., & Donnelly, R. J. 1995, *J. Low Temp. Phys.*, 100, 385
- Baym, G., Epstein, R., & Link, B. 1992, *Physica B*, 178, 1
- Bekarevich, I. L., & Khalatnikov, I. M. 1961, *Sov. Phys. JETP*, 13, 643
- Bell, J. B., & Colella, P. A. 1989, *J. Comput. Phys.*, 85, 257
- Bielert, F., & Stamm, G. 1993, *Cryogenics*, 33, 938
- Boyd, J. P. 2001, *Chebyshev and Fourier Spectral Methods* (Dover Publications)
- Brown, D. L., Cortez, R., & Minion, M. L. 2001, *J. Comput. Phys.*, 168, 464
- Canuto, C., Hussaini, M., Quarteroni, A., & Zang, T. 1988, *Spectral Methods in Fluid Dynamics* (Springer-Verlag)
- Chandler, E., & Baym, G. 1983, *J. Low Temp. Phys.*, 50, 57
- . 1986, *J. Low Temp. Phys.*, 62, 119
- Cheng, D. K., Cromar, M. W., & Donnelly, R. J. 1973, *Phys. Rev. Lett.*, 31, 433
- Chorin, A. J. 1968, *Math. Comp.*, 22, 745
- Dean, D. J., & Hjorth-Jensen, M. 2003, *Reviews of Modern Physics*, 75, 607
- Dimotakis, E. 1972, PhD thesis, California Institute of Technology
- Donati, P., & Pizzochero, P. M. 2003, *Physical Review Letters*, 90, 211101
- Donnelly, R. J. 1991, *Quantized Vortices in He II* (Cambridge University Press, Cambridge)
- Donnelly, R. J., & Barenghi, C. F. 1998, *J. Phys. Chem. Ref. Data*, 27, 1217
- Dumas, G., & Leonard, A. 1994, *J. Comp. Phys.*, 111, 205

- Fornberg, B. 1998, *A Practical Guide to Pseudospectral Methods* (Cambridge University Press, Cambridge)
- Germano, M., Piomelli, U., Moin, P., & Cabot, W. H. 1991, *Phys. Fluids*, 3, 1760
- Glaberson, W. I., Johnson, W. W., & Ostermeier, R. M. 1974, *Phys. Rev. Lett.*, 33, 1197
- Gorter, C. J., & Mellink, J. H. 1949, *Physica*, 85, 285
- Greenspan, H. P. 1968, *The Theory of Rotating Fluids* (Cambridge University Press, London)
- Greenstein, G. 1970, *Nature*, 227, 791
- Greenstein, G. 1974, in *IAU Symp. 53: Physics of Dense Matter*, 151–+
- Hall, H. E., & Vinen, W. F. 1956a, *Proc. R. Soc. Lond.*, A238, 204
- . 1956b, *Proc. R. Soc. Lond.*, A238, 215
- Henderson, K. L. 2001, *LNP Vol. 571: Quantized Vortex Dynamics and Superfluid Turbulence*, 571, 138
- Henderson, K. L., & Barenghi, C. F. 2000, *J. Fluid Mech.*, 406, 199
- Henderson, K. L., Barenghi, C. F., & Jones, C. A. 1995, *J. Fluid Mech.*, 283, 329
- Hills, R. N., & Roberts, P. H. 1983, *Arch. Rat. Mech. Anal.*, 66, 43
- Hobbs, G. 2002, PhD thesis, University of Manchester
- Hobbs, G., Lyne, A. G., Joshi, B. C., Kramer, M., Stairs, I. H., Camilo, F., Manchester, R. N., D’Amico, N., Possenti, A., & Kaspi, V. M. 2002, *MNRAS*, 333, L7
- Hobbs, G., Manchester, R., Teoh, A., & Hobbs, M. 2004, in *IAU Symposium*, 139–+
- Hollerbach, R. 1998, *Phys. Rev. Lett.*, 81, 3132
- Jones, P. B. 1998, *MNRAS*, 296, 217
- Khalatnikov, I. M. 1965, *Introduction to the Theory of Superfluidity* (Benjamin, New York)
- Landau, L. D., & Lifshitz, E. M. 1963, *Fluid Mechanics* (Pergamon Press, Massachusetts, USA)
- Levin, Y., & D’Angelo, C. 2004, *ApJ*, 613, 1157

- Lilly, D. K. 1992, *Phys. Fluids*, 4, 633
- Link, B. 2003, *Phys. Rev. Lett.*, 91, 101101
- Link, B., & Cutler, C. 2002, *MNRAS*, 336, 211
- Liu, M., Blohm, C., Egbers, C., Wulf, P., & Rath, H. J. 1996, *Phys. Rev. Lett.*, 77, 286
- Loukopoulos, V. C., & Karahalios, G. T. 2004, *Phys. Fluids*, 16, 2708
- Lyne, A. G., & Graham-Smith, F. 1998, *Pulsar Astronomy* (Cambridge University Press, Cambridge)
- Lyne, A. G., Shemar, S. L., & Smith, F. G. 2000, *MNRAS*, 315, 534
- Mahesh, K., Constantinescu, G., & Moin, P. 2004, *J. Comput. Phys.*, 197, 215
- Mamun, C. K., & Tuckerman, L. S. 1995, *Phys. Fluids*, 7, 80
- Marcus, P., & Tuckerman, L. 1987a, *J. Fluid Mech.*, 185, 1
- . 1987b, *J. Fluid Mech.*, 185, 31
- Mastrano, A., & Melatos, A. 2005, *MNRAS*(in press)
- McCulloch, P. M., Hamilton, P. A., McConnell, D., & King, E. A. 1990, *Nature*, 346, 822
- Mendell, G. 1991, *ApJ*, 380, 515
- Niemetz, M., Kerscher, H., & Schoepe, W. 2002, *J. Low Temp. Phys.*, 126, 287
- Orszag, S. A. 1974, *Mon. Weather Rev.*, 102, 56
- Ould Kaber, S. M. 1996, *J. Comput. Phys.*, 128, 165
- Rajagopal, K. 2002, in *AIP Conf. Proc. 610: Nuclear Physics in the 21st Century*, 147–156
- Reisenegger, A. 1993, *J. Low Temp. Phys.*, 92, 77
- Reisenegger, A., & Goldreich, P. 1992, *ApJ*, 395, 240
- Ruderman, M., Zhu, T., & Chen, K. 1998, *ApJ*, 492, 267
- Sauls, J. A. 1989, in *Timing neutron stars*, 4–15
- Schoepe, W. 2004, *Phys. Rev. Lett.*, 92, 095301

- Schwarz, K. 1988, *Phys. Rev. B*, 38 (4), 2398
- Sedrakian, A. 2005, *Phys. Rev. D*, 71, 083003
- Sedrakian, A. D., & Sedrakian, D. M. 1995, *ApJ*, 447, 305
- Sha, W., & Nakabayashi, K. 2001, *J. Fluid Mech.*, 431, 323
- Shemar, S. L., & Lyne, A. G. 1996, *MNRAS*, 282, 677
- Stairs, I. H., Lyne, A. G., & Shemar, S. L. 2000, *Nature*, 406, 484
- Streett, C. L., & Hussaini, M. Y. 1991, *Appl. Num. Math.*, 7, 41
- Swanson, C. E., Barenghi, C. F., & Donnelly, R. J. 1983, *Phys. Rev. Lett.*, 50, 190
- Thompson, C., & Duncan, R. C. 1993, *ApJ*, 408, 194
- Tilley, D. R., & Tilley, J. 1986, *Superfluidity and Superconductivity* (Adam Hilger Ltd, Bristol)
- Tsakadze, J. S., & Tsakadze, S. J. 1980, *J. Low Temp. Phys.*, 39, 649
- Tsubota, M., Araki, T., & Barenghi, C. F. 2003, *Phys. Rev. Lett.*, 90, 205301
- Tuckerman, L. S. 1983, PhD thesis, Massachusetts Institute of Technology
- Vandeven, H. 1991, *J. Sci. Comput.*, 6, 159
- Vinen, W. F. 1957, *Proc. R. Soc. London*, 242, 493
- Vollhard, D., & Wölfle, P. 2002, *The superfluid Phases of Helium 3* (Taylor & Francis, London)
- Weber, F., ed. 1999, *Pulsars as astrophysical laboratories for nuclear and particle physics*
- Wimmer, M. 1976, *J. Fluid Mech.*, 295, 317
- Yakovlev, D. G., Levenfish, K. P., & Shibano, Y. A. 1999, *Uspekhi Fizicheskikh Nauk*, 42, 737
- Yavorskaya, I. M., Belayev, Y. N., & Monakhov, A. A. 1975, *Sov. Phys. Dokl.*, 20 (4), 209

Table 1: Simulation Parameters

δ	Ω_2	Force type	Identifier
0.5	0.7	HV	Au
0.5	$0.7 \rightarrow 1$	HV	Aa
0.5	0.7	HV \rightarrow GM	Af
0.3	0.7	HV	Bu
0.3	$0.7 \rightarrow 1$	HV	Ba
0.3	0.7	HV \rightarrow GM	Bf
0.5	0.8	HV	Cu
0.5	$0.8 \rightarrow 1$	HV	Ca
0.5	0.8	HV \rightarrow GM	Cf
0.5	0.9	HV	Du
0.5	$0.9 \rightarrow 1$	HV	Da
0.5	0.9	HV \rightarrow GM	Df

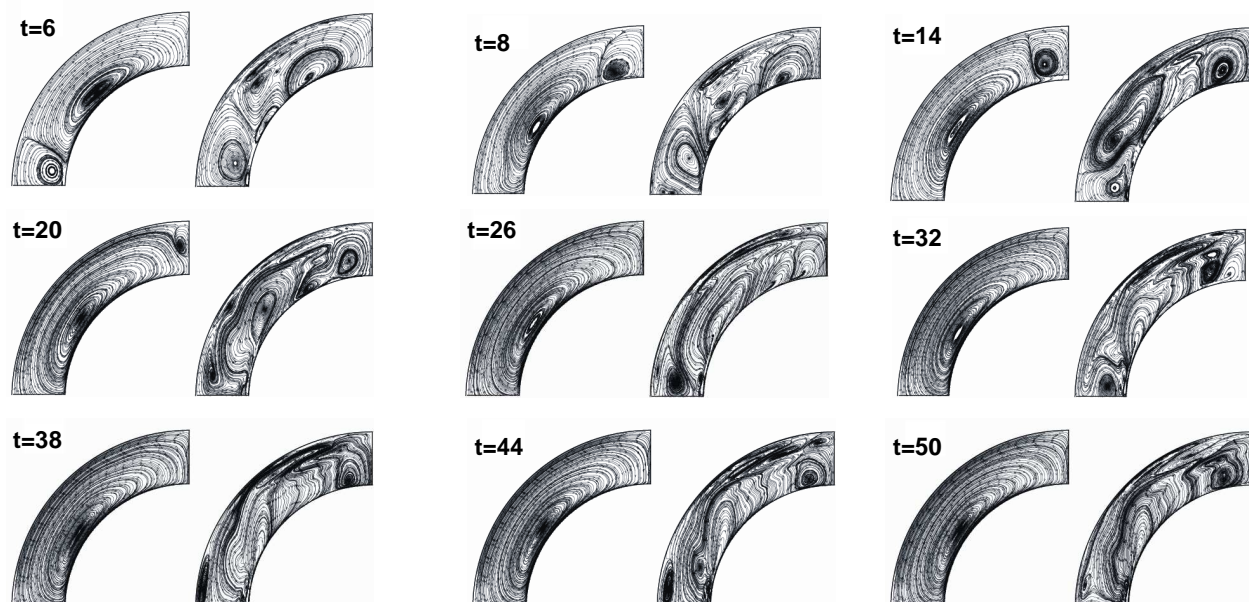


Fig. 1.— Meridional streamlines for the normal fluid (left) and the superfluid (right) as a function of time ($6 \leq t \leq 50$) for $\delta = 0.3$ and $\Delta\Omega = 0.3$ (case Bu, in Table 1). The time is expressed in units of Ω_1^{-1} .

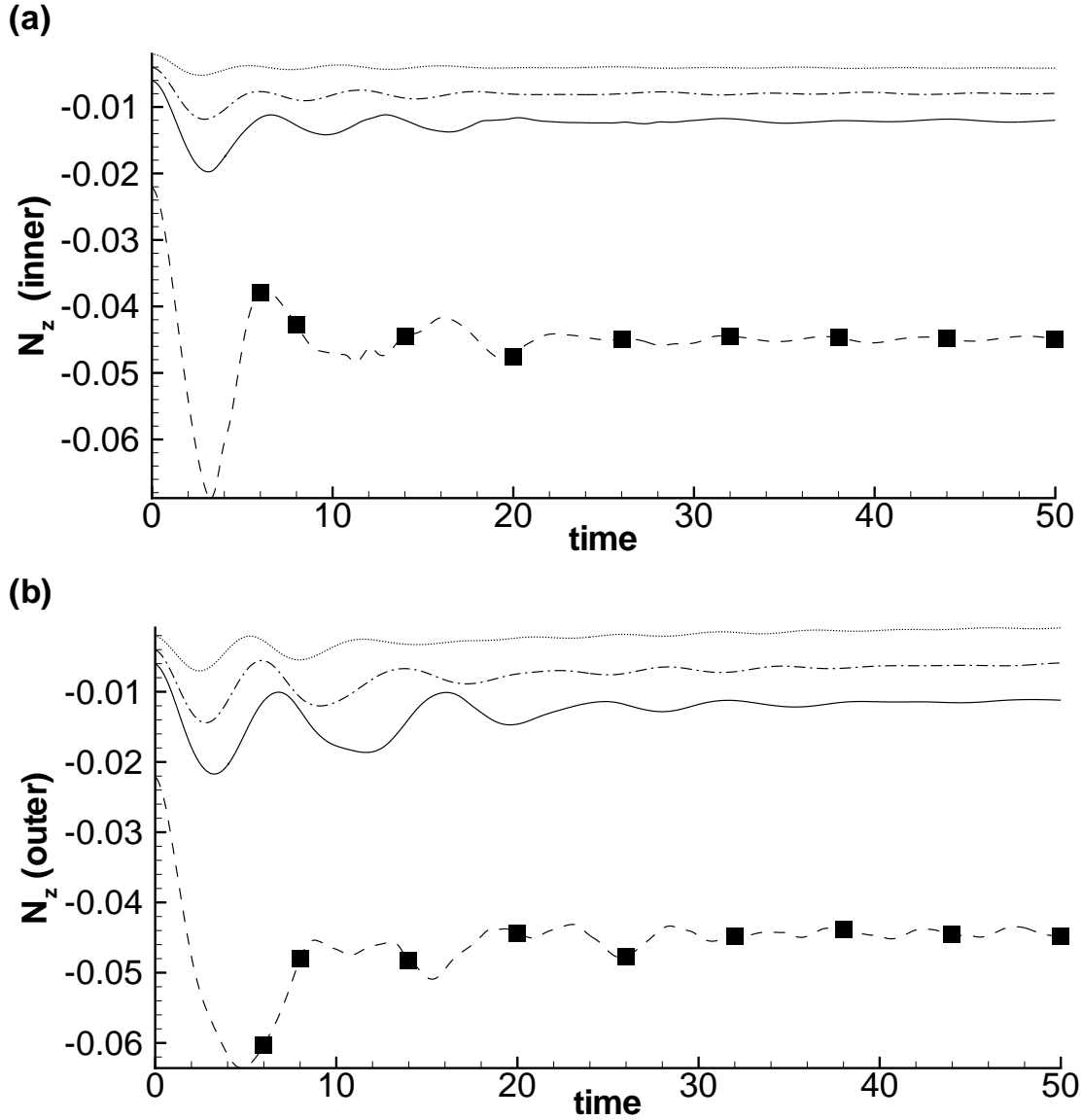


Fig. 2.— (a) Evolution of the (a) inner torque and (b) outer torque for the cases Au (solid curve), Bu (dashed curve), Cu (dash-dotted curve), and Du (dotted curve), whose parameters are quoted in Table 1. The time is expressed in units of Ω_1^{-1} and the torques in units of $\rho R_2^5 \Omega_2^2$. The filled squares correspond to the nine instantaneous snapshots of the streamlines plotted in Figure 1.

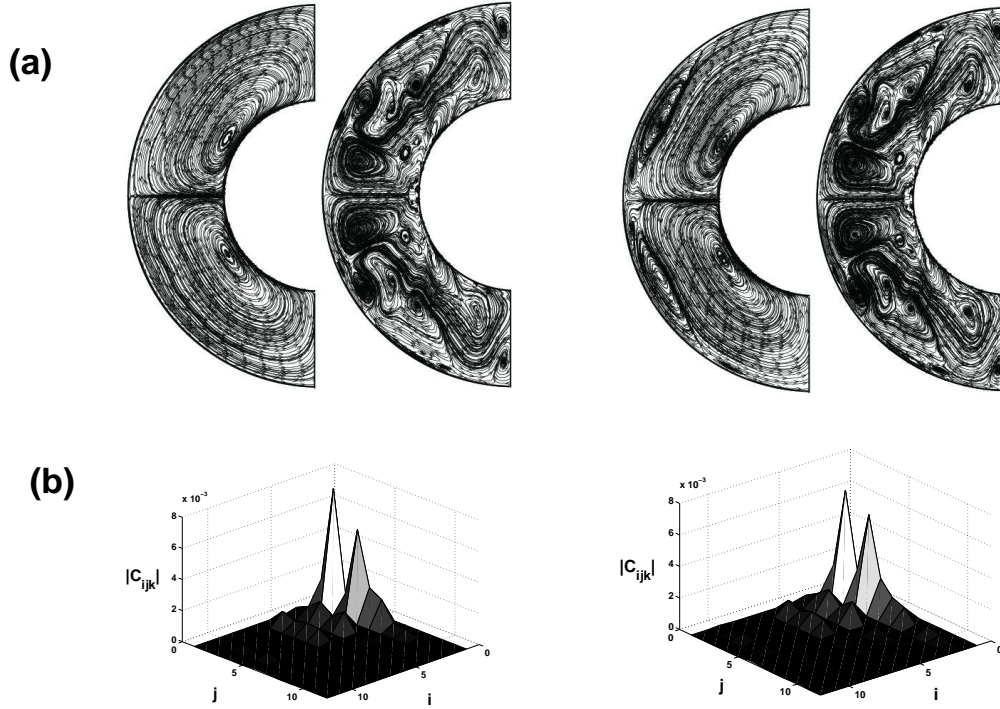


Fig. 3.— (a) Meridional streamlines before (left pair of hemispheres) and after (right pair of hemispheres) the outer sphere is accelerated instantaneously from $\Omega_2 = 0.7$ to $\Omega_2 = 1$ at $t = 20$. For each pair of hemispheres, the normal fluid streamlines are plotted at left and the superfluid streamlines are plotted at right. The results are for the case Af in Table 1. (b) Histograms of the magnitudes of the 12 dominant spectral coefficients of $(\mathbf{v}_n)_\theta$ before (left) and after (right) the acceleration at $t = 20$, as a function of the Chebyshev polynomial index i and the polar Fourier index j , with azimuthal index $k = 1$.

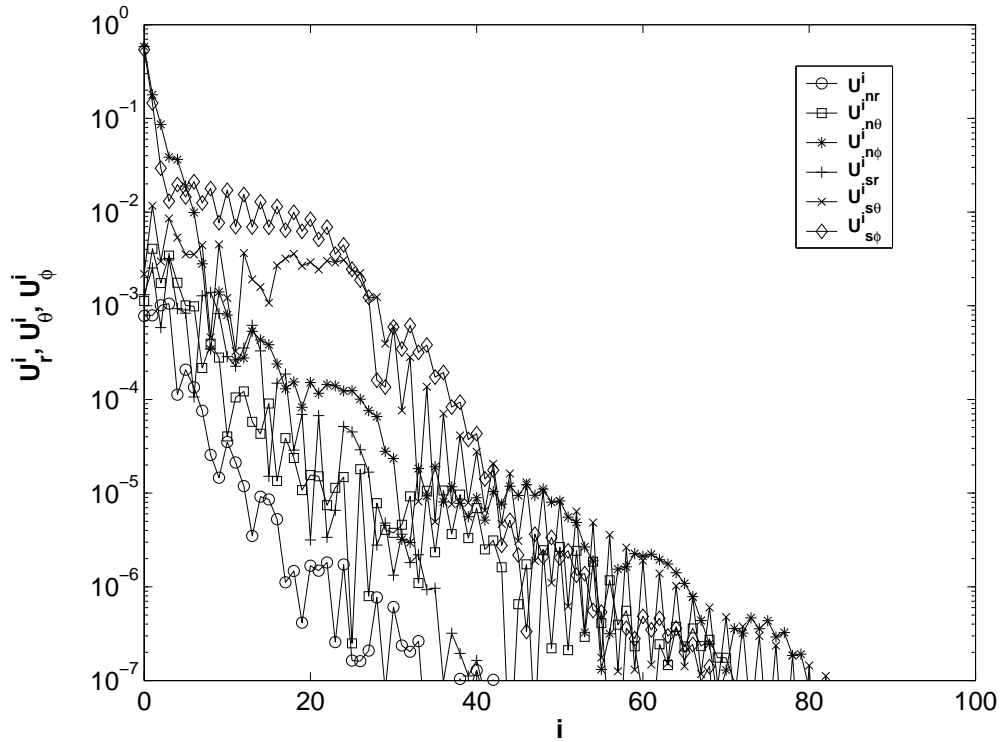


Fig. 4.— Modes amplitudes for the r (\circ), θ (\square), and ϕ ($*$) components of the normal fluid and the r ($|$), θ (\times), and ϕ (\diamond) components of the superfluid as a function of the Chebyshev polynomial index i , at $t = 20.1$. The results are for case Af in Table 1.

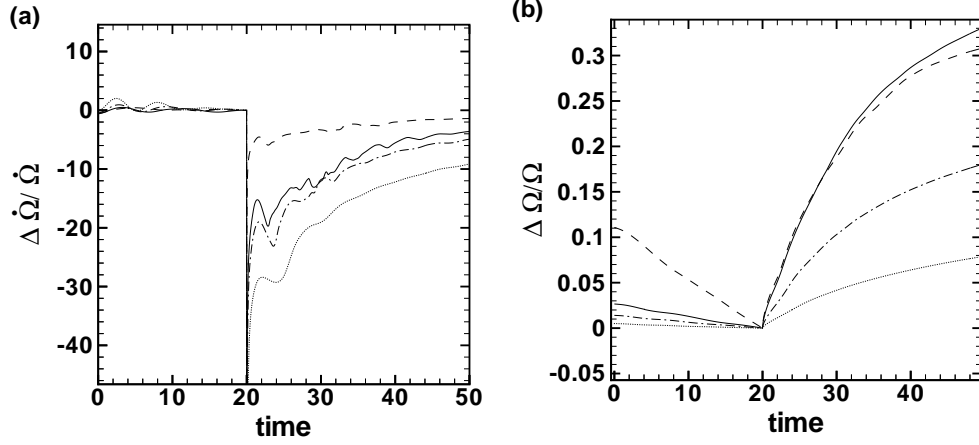


Fig. 5.— (a) Fractional change in angular acceleration of the outer sphere, $\Delta \dot{\Omega} / \dot{\Omega} = [\dot{\Omega}_2(t) - \dot{\Omega}_2(20)] / \dot{\Omega}_2(20)$, as a function of time. (b) Fractional change in angular velocity of the outer sphere, $\Delta \Omega / \Omega = [\Omega_2(t) - \Omega_2(20)] / \Omega_2(20)$, as a function of time. Time is measured in units of Ω_1^{-1} . Four cases are shown, whose parameters are quoted in Table 1: Aa (solid curve), Ba (dashed curve), Ca (dashed-dotted curve), and Da (dotted curve).

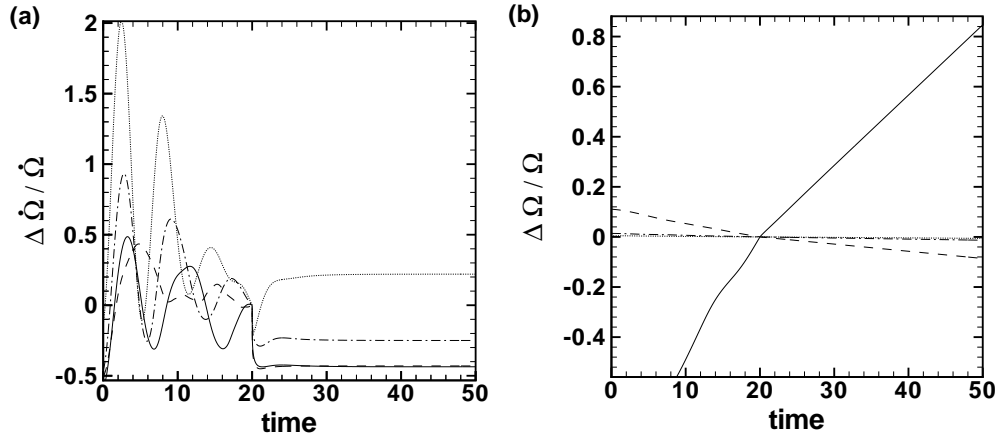


Fig. 6.— (a) Fractional change in angular acceleration of the outer sphere, $\Delta \dot{\Omega} / \dot{\Omega} = [\dot{\Omega}_2(t) - \dot{\Omega}_2(20)] / \dot{\Omega}_2(20)$, as a function of time. (b) Fractional change in angular velocity of the outer sphere, $\Delta \Omega / \Omega = [\Omega_2(t) - \Omega_2(20)] / \Omega_2(20)$, as a function of time. Time is measured in units of Ω_1^{-1} . Four cases are shown, whose parameters are quoted in Table 1: Af (solid curve), Bf (dashed curve), Cf (dashed-dotted curve), and Df (dotted curve).